Applied Catalysis A: General 495 (2015) 8–16

Contents lists available at ScienceDirect

Applied Catalysis A: General

journal homepage: www.elsevier.com/locate/apcata

Preparation of Ni–Mo–S catalysts by hydrothermal method and their hydrodeoxygenation properties

Weiyan Wang[a,b,*], Lu Li[a], Kui Wu[a], Kun Zhang[a], Jia Jie[a], Yunquan Yang[a,b,*]

[a] School of Chemical Engineering, Xiangtan University, Xiangtan, Hunan 411105, PR China
[b] National & Local United Engineering Research Centre for Chemical Process Simulation and Intensification, Xiangtan University, Xiangtan 411105, PR China

ARTICLE INFO

Article history:
Received 8 November 2014
Received in revised form 8 January 2015
Accepted 29 January 2015
Available online 7 February 2015

Keywords:
Ni–Mo–S
p-Cresol
Hydrodeoxygenation
Synergistic effect
Remote control model

ABSTRACT

Unsupported Ni–Mo–S catalysts with different Ni/(Ni + Mo) molar ratio were prepared by hydrothermal method using ammonium heptamolybdate and thiocarbamide as materials. The resultant catalysts were characterized by X-ray diffraction, nitrogen physisorption and transmission electron microscopy, and their activities were measured using the hydrodeoxygenation (HDO) of *p*-cresol as a probe reaction. The addition of Ni promoter caused a reduction in the surface area. The peaks attributed to NiS_2 on catalyst surface became noticeable as the Ni content increased in the catalyst. The catalyst with an optimal Ni/(Ni + Mo) molar ratio (0.3) exhibited the highest activity (99.8% deoxgenation degree at 300 °C and 4.0 MPa hydrogen pressure for 6 h). The HDO of *p*-cresol on these prepared Ni–Mo–S catalysts proceeded with two parallel routes: hydrogenation-dehydration (HYD) and direct deoxygenation (DDO), and HYD/DDO closely related to the Ni/(Ni + Mo) molar ratio in the catalyst, the HDO reaction temperature and H_2 pressure. The comparison of Ni–Mo–S with MoS_2–NiS_2 (prepared by two hydrothermal method) and $MoS_2 + NiS_2$ (prepared by physically mixing separately MoS_2 and NiS_2) indicated that the high HDO activity of Ni promoted MoS_2 catalyst was attributed to the synergistic effect of MoS_2 and NiS_2 rather than the formation of Ni–Mo–S phase, which could be well explained by the remote control model.

1. Introduction

The continuous decrease in fossil fuels reserves, rapid growth in global energy consumption and stringent environmental regulations in greenhouse gases emissions have attracted much attention in the development of renewable energy resource in the last ten years [1,2]. Bio-oil, derived from biomass by fast pyrolysis, is a promising substituted fuel because of the CO_2-neutral and free of SOx emission during its combustion. Unfortunately, this bio-oil contains a considerable amount of oxygenated compounds such as phenols, aldehydes, ketones and furans, contributing to its high oxygen content, which leads to some deleterious properties and prevents its direct utilization as a supplement or replacement for gasoline or fossil diesel [3,4]. Consequently, upgrading bio-oil to liquid hydrocarbon via catalytic hydrodeoxygenation (HDO) becomes a challenge for obtaining renewable, sustainable and environment friendly liquid fuel, and the key to this technology is how to prepare HDO catalysts with high activity.

Some investigators had studied the HDO of the biomass-derived oils on sulfides and noble metal catalysts [5,6]. Because of the intermolecular interaction and adsorption-site competition in a complex mixture such as bio-oils, detailed study with model compound is of significance for understanding the different reaction paths and reaction mechanism [7]. Phenols are widely selected as model compounds to investigate the HDO activity of various catalysts under different conditions [8–22] since they take a considerable quantity in bio-oil (66.9%) [23] and possess a high C—O bond dissociation energy [2,24]. The HDO of these phenols usually occurs via two main pathways: direct deoxygenation (DDO) with aromatic C—O bond scission and hydrogenation-dehydration (HYD) that starts with ring hydrogenation followed by dehydration reactions. Among these catalysts that applied in the HDO of phenols, noble metals and amorphous Mo(W) based borides exhibit high activities, but the high cost or insufficient stability at high temperature inhibit their widely practical application. Ni or Co promoted Mo- or W-based sulfide catalysts are usually prepared by sulfidation of oxide precursors at high temperature (about 400 °C) with H_2/H_2S or organic sulfur compound [20]. This method requires H_2S or releases poisonous gas and causes

---

* Corresponding authors at: School of Chemical Engineering, Xiangtan University, Xiangtan, Hunan 411105, PR China. Tel.: +86 731 58298581; fax: +86 731 58293284.
E-mail addresses: wangweiyan@xtu.edu.cn (W. Wang), yangyunquan@xtu.edu.cn (Y. Yang).

http://dx.doi.org/10.1016/j.apcata.2015.01.041
0926-860X/© 2015 Elsevier B.V. All rights reserved.

some agglomeration. To overcome these disadvantages on the synthesis of sulfide catalyst, several new methods such as thermal decomposition method [25], mechanical activation method [26] and hydrothermal method [17] had appeared. As we known, the synthesis method has a great effect for the performance of catalyst. For instance, Smith et al. [22] had prepared MoS_2 catalysts by different methods and compared their activities based on kinetic study. They found that exfoliated MoS_2 had the highest activity in the HDO of phenols. Wang et al. [26] had adopted mechanical activation method to prepare Ni–Mo–W sulfide catalysts and confirmed that these catalysts had high catalytic activity for the HDO of *4*-methylphenol. Hydrothermal method, an important technique for producing highly homogeneous nano-composite materials, has become one of the most efficient processes for the preparation of nano-catalyst. Adopting the isolation effect of the organic solvent for the precursor molecules, Yoosuk et al. [27] had prepared unsupported Mo based sulfide catalyst with a surface area in the range of 138–368 m^2/g and found that MoS_2 catalyst prepared by the hydrothermal method showed 2.4-fold higher conversion than commercial crystalline MoS_2 in the HDO of phenol [17].

To explain the active sites for Ni(Co) promoted MoS_2 catalysts, there had proposed several models. Two generally accepted models are Co(Ni)–Mo–S model and remote control (RC) model. Co(Ni)–Mo–S model claims that the effect of Co or Ni in Mo sulfide catalyst is attributed to the location of promoter atom on the edges of MoS_2 layers [28]. RC model supposes that the spillover hydrogen migrates from a donor phase (such as Co_9S_8 and NiS_x) to an acceptor phase (such as MoS_2, WS_2 and ReS_2) and modifies the latter. Gil-Llambías et al. [29–31] had provided a direct proof of the role of a remote control in the hydrodesulfurization using a reactor with physically separated and layered catalyst beds. As we known, all of literatures reported that the high activity of $Co(Ni)MoS_2$ catalysts in the HDO is attributed to the formation of Co(Ni)–Mo–S phase [17,27]. However, the stability of the so-called Co(Ni)–Mo–S phase decreases if the reaction temperature increases [32], and this phase will decompose during the reaction [33,34], suggesting that Co(Ni)–Mo–S phase is only a 'precursor' of the real catalyst system [30]. Hence, the explanation of the exact nature of active sites by Co(Ni)–Mo–S model is still a subject of debate. In this work, we prepare unsupported Ni–Mo sulfide catalysts by hydrothermal method used ammonium heptamolybdate and thiocarbamide as initial materials. The first aim is to obtain the maximum deoxygenation degree in the HDO of *p*-cresol by studying the effects of Ni content on the catalytic activity and the HDO reaction conditions on the conversion and product distribution in detail. The additional one is to reveal the HDO reaction mechanism by comparing the HDO activity of different Ni–Mo–S catalysts with the same Ni–Mo molar ratio.

2. Experimental

2.1. Catalyst preparation

All solvents and reagents were obtained from Sinopharm Chemical Reagent Co., Ltd. in high purity (≥99%) and used without further purification. Unsupported Ni–Mo–S catalysts were synthesized by using one step hydrothermal method. The catalyst synthesis was carried out in quartz reactor with a volume of 300 mL. Nickel nitrate, ammonium heptamolybdate (2.3 g) and thiourea (3.0 g) were dissolved in 250 mL ultra-pure water. The composition of the samples was adjusted by changing the initial Ni/Mo molar ratio in the solution. The mixed solution was added into a reactor, and then sealed and heated to 200 °C. After 24 h, the resulting catalysts were separated and washed with absolute ethanol several times to remove the residual water and water-soluble impurities. Finally, the resulting product was dried under vacuum at 50 °C for 8 h and stored in nitrogen environment. The prepared catalysts were denoted as Ni–Mo–*X*, where *X* represented the molar ratio of Ni/(Ni + Mo) in the initial solution.

2.2. Catalyst characterization

X-ray diffraction (XRD) measurements were carried on a *D*/max2550 18 kW Rotating anode X-ray Diffractometer with monochromatic Cu Kα radiation ($\lambda = 1.5418$ Å) radiation at voltage and current of 40 kV and 300 mA. The 2θ was scanned over the range of 10–90° at a rate of 10°/min. The specific surface area was measured by a Quantachrome's NOVA-2100e Surface Area instrument by physisorption of nitrogen at −196 °C. The samples were dehydrated at 300 °C using vacuum degassing for 12 h before physical absorption experiments. The morphologies of catalysts were determined by transmission electron microscopy (TEM) on a JEOL JEM-2100 transmission electron microscope with a lattice resolution of 0.19 nm and an accelerating voltage of 200 kV. The samples for the TEM study were prepared by the ultrasonic dispersing in ethanol and consequent deposition of the suspension upon a "holey" carbon film supported on a copper grid. The samples were kept under inert atmosphere until the last process.

2.3. Catalyst activity measurement

The HDO activity tests were carried out in a 300-mL sealed autoclave with the inner diameter of 50 mm, height of 185 mm and vessel walls thickness of 7 mm. The prepared catalyst without any further treatment (0.60 g), *p*-cresol (13.50 g) and dodecane (86.50 g) were placed into the autoclave. Air in the autoclave was evacuated by pressurization–depressurization cycles with nitrogen and subsequently with hydrogen. The system was heated to the required temperature with a heat-up rate of 10 °C/min and kept constant, then pressurized with hydrogen to 4.0 MPa and adjusted the stirring speed to 900 rpm. During the reaction, liquid samples were withdrawn from the reactor and analyzed by Agilent 6890/5973 N GC–MS and 7890 gas chromatography using a flame ionization detector (FID) with a 30 m AT-5 capillary column. To separate the reaction products, the temperature in the GC oven was heated from 40 °C to 85 °C with the ramp of 20 °C/min, held at 85 °C for 4.0 min, then heated to 200 °C at a rate of 20 °C/min and kept at 200 °C for 5.0 min. Internal standards (i.e., octane for methylcyclohexane, toluene and decane for *p*-cresol) were used to determine the product distribution and carbon balance. The experiments have been repeated twice at least and the results showed that the conversion and selectivity were within 3.0% of the average values. The carbon balance in the sample for each of experiment was better than 95.0 ± 3.0%. The conversion, selectivity, deoxygenation degree and HYD/DDO for each experiment were calculated as follows:

$$\text{Conversion(mol\%)} = \left(1 - \frac{\text{moles of residual reactant}}{\text{moles of initial reactant}}\right) \times 100\%$$

$$\text{Selectivity(A, mol\%)} = \frac{\text{moles of product(A)}}{\text{moles of reacted reactant}} \times 100\%$$

$$\text{Deoxygenation degree(D.D.,wt\%)} = \left(1 - \frac{\text{oxygen content in the final organic compounds}}{\text{total oxygen content in the initial material}}\right) \times 100\%$$

$$\frac{\text{HYD}}{\text{DDO}} = \frac{\text{total selectivity of methylcyclohexane and 4-methylcyclohexene}}{\text{selectivity of toluene}}$$

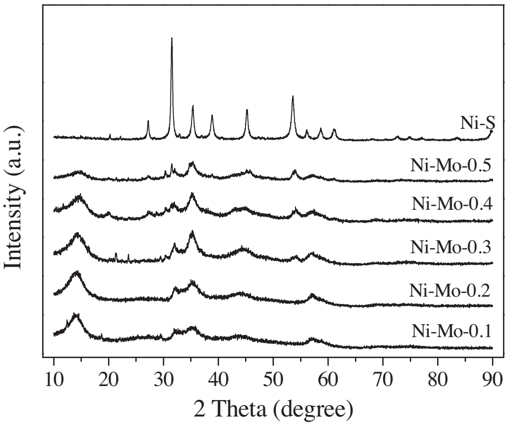

Fig. 1. XRD patterns of Mo–S, Ni–Mo–S and Ni–S samples.

We compared the conversion and product selectivity at different time under the same conditions except for the stirring rate (700 r/min and 900 r/min). The effect of the particle size on catalytic activity was also studied. The results showed the external mass transfer limitation in the sealed autoclave with a high stirring rate (900 r/min) was negligible and the reaction was under kinetic control with no internal diffusion limitations under the investigated conditions. Previous literatures [21,35] claimed that the decomposition of *p*-cresol is modeled assuming a pseudo-first-order reaction ($\ln(1-x) = -k\cdot C_{cat}\cdot t$), the reaction rate constant (k, mL/(s g catalyst)) was g to the change of conversion (x) with reaction time (t, s).

2.4. Characterization of the amorphous catalysts

2.4.1. XRD studies

The XRD patterns of the prepared Ni–Mo–S catalysts with different Ni/(Ni + Mo) molar ratio are shown in Fig. 1. Compared with the crystalline MoS_2, all the unsupported Ni–Mo–S catalysts exhibited some broad diffraction peaks at $2\theta = 14°$, 33°, 39°and 59°, indicating a poorly crystalline structure characteristic of MoS_2 [36]. The XRD pattern of Ni–S presented several sharp peaks at $2\theta = 27°$, 31°, 35°, 38°, 45°, 53°, assigning to NiS_2 (JCPDS Card No. 01-088-1709) [37]. The peaks at $2\theta = 14°$ and 59° corresponded to the (0 0 2) and (1 1 0) planes of MoS_2, respectively [38]. Of these two peaks, the intensity of the (0 0 2) peak at $2\theta = 14°$ represented the multi-stacked slabs along the *c*-axis while the intensity of the (1 1 0) peak at $2\theta = 59°$ represented the layer of the slabs [25]. As shown in Fig. 1, the intensity of the (0 0 2) peak increased firstly and then decreased gradually with the Ni/(Ni + Mo) molar ratio. When the Ni/(Ni + Mo) molar ratio was lower than 0.3, except for some broad diffraction peaks that attributed to MoS_2, no obviously peaks for nickel sulfides were observed, indicating that nickel sulfides might be highly dispersed on MoS_2 or existed in very small nano-crystallites. Previous study had attributed this unobserved nickel sulfide species in the XRD pattern to the formation of Ni–Mo–S phase, which overlapped the diffraction peaks from MoS_2 [39], but this needed to be further verified. Some diffraction peaks at $2\theta = 31°$, 35°, 45° and 53° that assigned to NiS_2 were observed in the XRD patterns of Ni–Mo–0.3, Ni–Mo–0.4 and Ni–Mo–0.5. These NiS_2 peaks became noticeable and sharp with the increase of Ni content, suggesting that there produced more NiS_2 on the catalyst surface.

2.4.2. HRTEM studies

Fig. 2 shows the high resolution transmission electron microscopy (HRTEM) micrographs of Mo–S, Ni–Mo–0.2, Ni–Mo–0.3, Ni–Mo–0.5 and Ni–S samples. Some groups of parallel black thread-like fringes presented clearly in Mo–S, Ni–Mo–0.2, Ni–Mo–0.3 and Ni–Mo–0.5 images. The spacing between these fringes was about 0.65 nm, characterizing the (0 0 2) basal planes of crystalline MoS_2 [20,27,38]. Ni–S image displayed some parallel fringes with a spacing of about 0.26 nm, which matched well with the distance between the (2 0 0) crystal planes of NiS_2. Qualitative analysis revealed that Ni–Mo–0.2 catalyst had 4–7 stacked layers and the slab length of fringes reaches up to 30 nm. The stacking degree of Ni–Mo–0.3 was determined to be about 7 slabs and the length of most slabs was lower than 10 nm. Ni–Mo–0.5 showed a stacking of 2–5 layers with an average length about 5 nm. This indicated that the slab length of MoS_2 was shorted by adding Ni. In the HRTEM image of Ni–Mo–0.5, except for the lattice fringes of MoS_2, some other parallel fringes with a distance of 0.26 nm that covered on MoS_2 fringes could also be seen, This suggested that nickel sulfide species on the catalyst surface was enough to be detected when the Ni content increased above a certain threshold nickel concentration level, which agreed well with the XRD analysis and other investigations [26,27].

2.4.3. Nitrogen sorption studies

The specific surface area, pore volume and pore size of the Mo–S, Ni–Mo–S and Ni–S unsupported catalysts prepared by hydrothermal method without organic solvent are summarized in Table 1. Unlike the reports [27,39] that Ni–Mo–S catalysts had a surface area in the range of 138–329 m^2/g and pore volume in the range of 0.55–0.77 cm^3/g, in this study, the surface of MoS_2 catalyst without adding any Ni was only 79.8 m^2/g. This was resulted from the different synthesis methods. The method in the literatures [27,39] adopted the dispersion effect of organic solvent to distribute the precursor molecules and prevent the produced particle from agglomeration in some extent during preparation. But the method in our study used water as a solvent, leading to the particles agglomeration and the low surface area of the resultant samples. Ni content had significant effects on the specific surface area and pore volume of these sulfide catalysts. When increasing the Ni/(Ni + Mo) molar ratio from 0.1 to 0.5, the specific surface area decreased from 40.4 m^2/g to 10.8 m^2/g and the pore size reduced to 3.8 nm. Because of the excess deposition of NiS_2 species on MoS_2, the textural properties of Ni–Mo–S changed very little when Ni/(Ni + Mo) molar ratio was increased from 0.4 to 0.5. This negative effect of Ni promoter mainly resulted from the uniform insertion of nickel sulfide particles with low surface area in the pore channels of the MoS_2 phase layer [25]. This phenomenon has also been found in the previous investigations [17,39].

2.5. Catalytic activity

2.5.1. HDO of *p*-cresol on Mo–S and Ni–Mo–S unsupported catalysts

The catalytic performances of Ni–Mo–S catalysts were tested using the HDO of *p*-cresol as the probe reaction. As shown in Fig. 3, the products in the HDO of *p*-cresol on Mo–S and Ni–Mo–0.3 at 300 °C were toluene, 4-methylcyclohexene and methylcyclohexane, and no oxygen-containing compound was detected, which indicated that these Ni–Mo–S catalysts possessed a high deoxygenation activity under the studied conditions. The concentration profiles as a function of time showed that *p*-cresol concentration decreased gradually while both the methylcyclohexane concentration and toluene concentration increased. Fig. 3a shows that toluene concentration was 4 times larger than methylcyclohexane concentration, suggesting that DDO was the primary reaction route for the HDO of *p*-cresol on Mo–S catalyst. When promoter Ni was added into Mo–S, the HDO activity was improved, and the product distribution was also changed. The end product concentration decreased in the order of 4-methylcyclohexane > toluene >

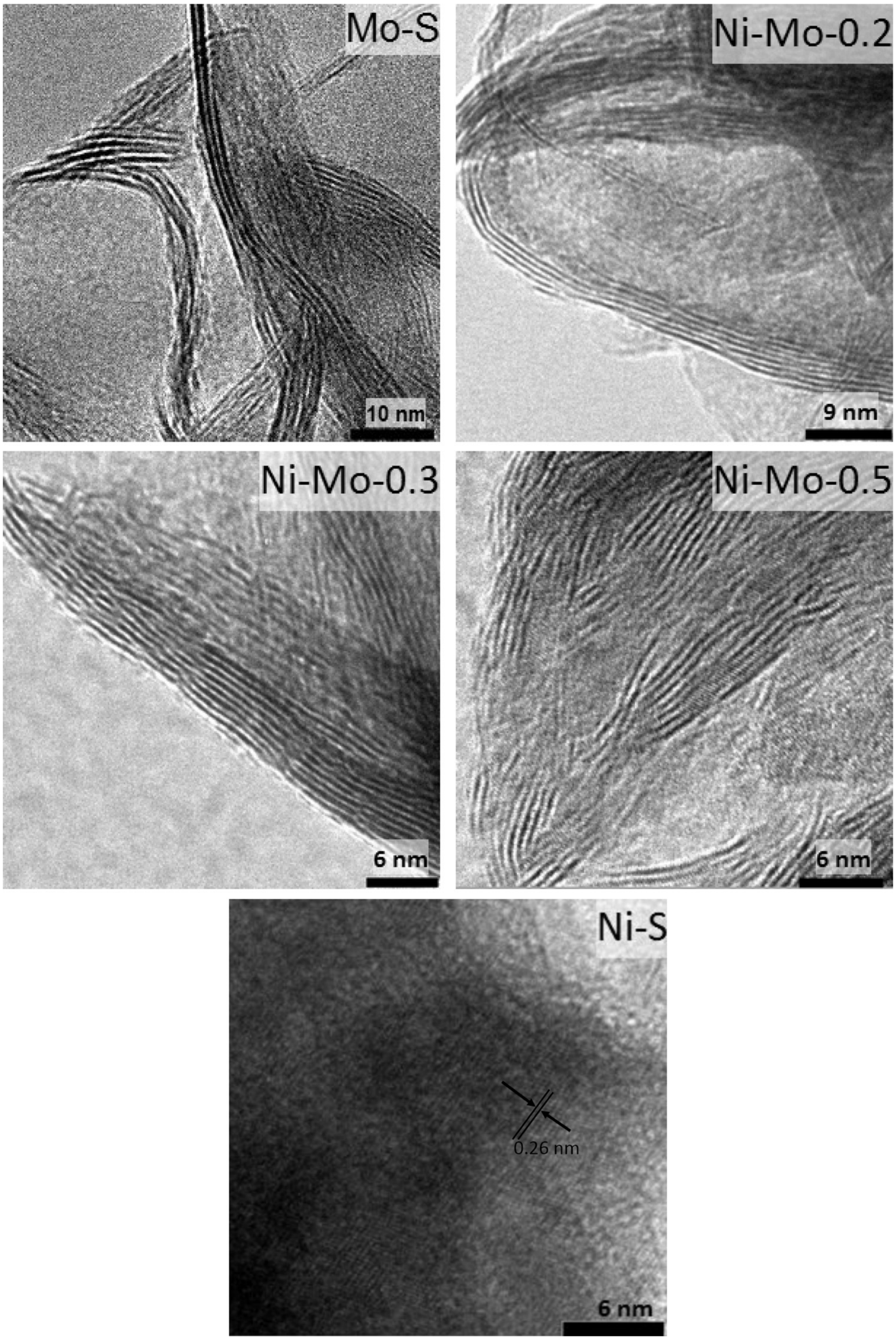

Fig. 2. HRTEM images of Mo–S, Ni–Mo–0.2, Ni–Mo–0.3, Ni–Mo–0.5 and Ni–S samples.

Table 1
Physical properties of Mo–S and Ni–Mo–S unsupported catalysts.

Catalysts	Ni/(Ni + Mo)	Surface area (m^2/g)	Pore volume (cm^3/g)	Pore size (nm)
Mo–S	0	79.8	0.4	3.0, 12.0
Ni–Mo–0.1	0.1	40.4	0.2	8.8
Ni–Mo–0.2	0.2	25.8	0.1	7.2
Ni–Mo–0.3	0.3	16.3	0.1	6.5
Ni–Mo–0.4	0.4	10.7	0.1	3.8
Ni–Mo–0.5	0.5	10.8	0.1	3.8
Ni–S	1	10.2	0.1	2.4

Table 2
Activity and selectivity of unsupported Ni–Mo–S catalysts for the HDO of *p*-cresol at 300 °C for 6 h.

Catalyst	Without catalyst	Mo–S	Ni–Mo–0.1	Ni–Mo–0.2	Ni–Mo–0.3	Ni–Mo–0.4	Ni–Mo–0.5	Ni–S
Conversion, mol %	19.0	67.0	79.4	97.4	99.9	92.6	87.6	32.4
$k \times 10^2$ mL/(s g catalyst)	0.2	1.1	1.5	2.5	3.2	2.1	1.7	0.4
Product selectivity, mol %								
Methylcyclohexane	9.9	24.8	58.1	64.6	67.1	68.9	69.3	32.3
3-Methylcyclohexene	4.1	1.1	2.3	2.78	4.12	4.99	5.23	12.1
Toluene	86.0	74.1	39.3	32.6	28.8	26.2	25.5	55.6
HYD/DDO	0.2	0.4	1.6	2.1	2.5	2.8	2.9	0.8
D.D., wt %	16.8	63.7	77.2	97.1	99.8	91.8	86.2	29.5

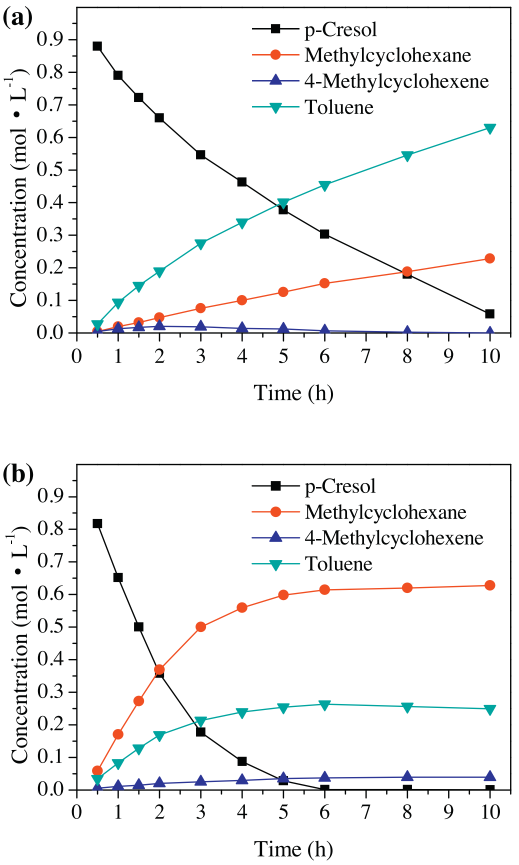

Fig. 3. The concentration changes of *p*-cresol and product versus reaction time on (a) Mo–S and (b) Ni–Mo–0.3 catalysts. Reaction condition: pressure 4.0 MPa, temperature 300 °C, stirring rate 900 r/min.

4-methylcyclohexene. The HYD/DDO on Ni–Mo–S was much higher than that on Mo–S, which suggested that adding promoter Ni into Mo–S was favorable to the HYD route to produce methylcyclohexane. It has been demonstrated that some cyclohexanol or cyclohexanone analogs as intermediates in small amount were formed via hydrogenation of the corresponding aromatic ring before the C—O σ-bond scission [17,27,40], but not any 4-methylcyclohexanol was detected in this work. However, the HDO of *p*-cresol cannot produce methylcyclohexane within one step. For the HYD route, *p*-cresol is hydrogenated to 4-methylcyclohexanol at first and then deoxygenated to methylcyclohexane. This is a consecutive reaction, in which 4-methylcyclohexanol acts as an intermediate. After 6 h at 300 °C, as shown in Table 2, the total selectivity for methylcyclohexane and 4-methylcyclohexene was higher than 60.0%, but not any 4-methylcyclohexanol was found during the reaction. Therefore, the hydrogenation of *p*-cresol to 4-methylcyclohexanol prior to the deoxygenation step was concluded to be the rate-limiting step in the HDO of *p*-cresol on Ni–Mo–S catalysts.

The activity of Mo–S, Ni–Mo–S and Ni–S catalysts in the HDO of *p*-cresol is summarized in Table 2. For comparison, the HDO of *p*-cresol without catalyst was also studied. After 6 h at 300 °C, the conversion was 19.0% and the HYD/DDO was 0.2. When adding Mo–S catalyst in the reaction system, the conversion increased to 67.0% with a deoxygenation degree of 63.7%. With the increase of Ni content in Ni–Mo–S catalyst, *p*-cresol conversion went up to 99.9% on Ni–Mo–0.3 and then decreased to 87.6% on Ni–Mo–0.5. The selectivity of methylcyclohexane yielded by HYD route increased in the order of Mo–S (24.1%) < Ni–Mo–0.1 (58.1%) < Ni–Mo–0.2 (64.6%) < Ni–Mo–0.3 (67.1%) < Ni–Mo–0.4 (68.9%) < Ni–Mo–0.5 (69.3%). The *p*-cresol conversion on Ni–S was only 32.4% with a deoxygenation degree of 29.5% under the same conditions, showing its low HDO activity. However, the characterization results showed that NiS_2 on the catalyst surface increased with Ni content, which covered on some MoS_2 active sites. Consequently, the reduction of activity at high content of Ni was attributed to the coverage of active sites by NiS_2.

The reaction rate constant (*k*) for Mo–S, Ni–Mo–0.1, Ni–Mo–0.2, Ni–Mo–0.3, Ni–Mo–0.4, Ni–Mo–0.5 and Ni–S were 1.1, 1.5, 2.5, 3.2, 2.05, 1.7 and 0.4×10^{-2} mL/(s g catalyst), respectively. For comparison, Ni–Mo–S/γ-Al_2O_3 (γ-Al_2O_3, 156.2 m^2/g), as a traditional and industrial catalyst, was prepared as described in the previous literature [41] and applied into the HDO of *p*-cresol. The final deoxygenated products were the same as that on Ni–Mo–*X* catalysts. After reacting at 300 °C for 10 h, the conversion was only 47.1% with a selectivity of 39.4% toluene and a deoxygenation degree of 44.1%. The calculated reaction rate constant (*k*) for Ni–Mo–S/γ-Al_2O_3 was 0.4×10^{-2} mL/(s g catalyst), which was much smaller than that for Ni–Mo–S under the same reaction conditions. Compared with the other catalyst preparation methods, in this study, the Ni–Mo–S prepared by hydrothermal method did not require high temperature and any H_2 or inert gas, showing its superiority on the operation. In addition, Ni–Mo–S showed high HDO activity, which was higher than other catalysts in previous literatures based on the comparison of reaction rate constant (*k*) [13,21,22,42]. For the HDO reaction on these sulfides catalyst, sulfur was inevitable to remove from catalyst under high temperature and high pressure of hydrogen [48]. Mo-based sulfides catalyst also possesses high HDS activity [49,50]. Adding an appropriate amount of S-containing compound such as thiophene in the HDO reaction system can efficiently inhibit the removal of sulfur and then decline the catalyst deactivation rate.

2.5.2. *Effect of temperature and pressure on HDO of p-cresol*

The effects of reaction temperature on the conversion and selectivity of products in the HDO of *p*-cresol on Ni–Mo–0.3 catalyst were studied at a constant pressure of 4.0 MPa and stirring rate of 900 r/min. The results, as shown in Fig. 4, indicated that the *p*-cresol conversion significantly increased with temperature and the product distribution also displayed noticeable temperature dependence. The conversion of *p*-cresol was 59.6% at 250 °C, which increased to 96.8% as temperature increased to 325 °C. The tendency of the change in conversion as the reaction temperature indicated that this HDO reaction was highly influenced by kinetics.

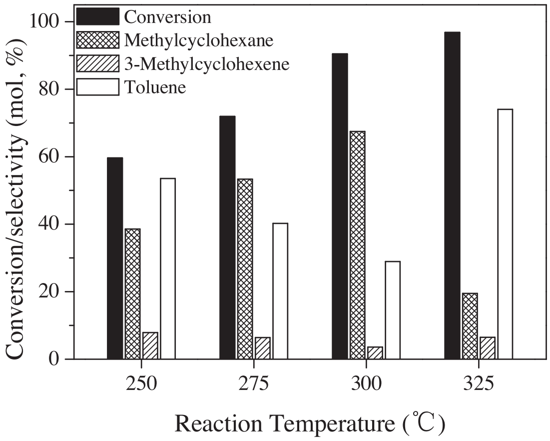

Fig. 4. HDO of *p*-cresol on Ni–Mo–0.3 catalyst at different reaction temperature. Reaction condition: pressure 4.0 MPa, reaction time 4 h, stirring rate 900 r/min.

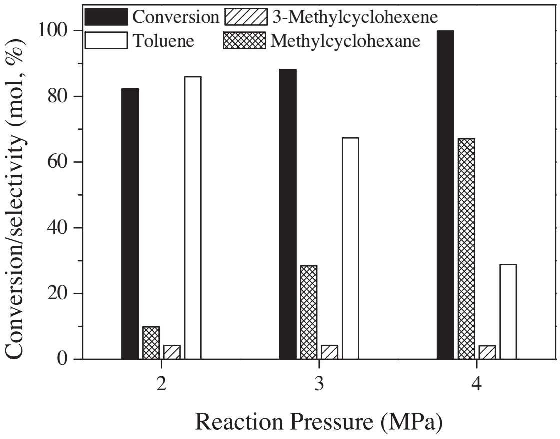

Fig. 5. HDO of *p*-cresol on Ni–Mo–0.3 catalysts at different reaction pressure. Reaction condition: temperature 300 °C, reaction time 6 h and stirring rate 900 r/min.

The methylcyclohexane selectivity was 38.6% at 250 °C and reached a maximum (67.5%) at 300 °C and finally decreased to 19.5% at 325 °C, while the toluene selectivity decreased from 53.5% to 28.9% and then increased rapidly to 74.0% when the temperature was varied from 250 °C to 325 °C. The corresponding HYD/DDO ratios on Ni–Mo–0.3 catalyst at 250 °C, 275 °C, 300 °C and 325 °C were 0.9, 1.5, 2.5 and 0.4, respectively, indicating that the HYD route was enhanced as temperature increased to 300 °C and then the direct deoxygenation route was greatly promoted when the temperature was further increased to 325 °C.

The great change on the product distribution at different reaction temperature can be explained as following two reasons. On the one hand, according to the products, some key reactions and the corresponding Gibbs free energy of each reaction as a function of the temperature is analyzed and given in Table 3. The direct deoxygenation reaction (R1) was possible in the measuring range of temperature, but the formation of methylcyclohexane from *p*-cresol was not favored because the Gibbs free energy for R4 was a positive value when the temperature was higher than 300 °C, leading to an obvious increase of toluene. Compared with the Gibbs free energies for R3 and R6 at 300 °C and 325 °C, it could be concluded that the hydrogenation of *4*-methylcyclohexene to methylcyclohexane was harder than the conversion of *p*-cresol to *4*-methylcyclohexene, and this case became more serious at 325 °C, causing the higher selectivity of 4-methylcyclohexene at 325 °C than at 300 °C. On the other hand, Faglioni and Goddard [43] have reported that H_2 surface coverage over the catalyst increased with H_2 pressure but decreased with temperature because of the different solubility of hydrogen in the solvent. Therefore, the available H_2 on the catalyst surface might be sufficient at 300 °C, favoring the HYD pathway to form methylcyclohexane, but when the temperature was increased to 325 °C, the H_2 adsorbed on the catalyst surface was unsaturated, leading to a selectivity shift toward to toluene.

Fig. 5 shows the HDO of *p*-cresol on Ni–Mo–0.3 catalysts at different reaction pressure and 300 °C for 4 h. It was observed that the hydrogen pressure had a great effect on the conversion and product selectivity. When increasing the hydrogen pressure from 2.0 MPa to 4.0 MPa, the *p*-cresol conversion increased from 82.3% to 99.8%, while the toluene selectivity decreased from 85.9% to 28.8%. The HYD/DDO ratios on Ni–Mo–0.3 catalyst at a total pressure of 2.0 MPa, 3.0 MPa and 4.0 MPa were 0.2, 0.5 and 2.5, respectively. This suggested that increasing hydrogen pressure was favorable for the HYD route, which mainly related to the hydrogen solubility. Increasing hydrogen pressure could improve the hydrogen solubility in liquid phase. Correspondingly, the hydrogen concentration absorbed on Ni–Mo–0.3 catalyst surface was enhanced. After the adsorption of *p*-cresol on Ni–Mo–0.3 catalyst, the hydrogenation of the aromatic ring became dominant under the high concentration of hydrogen on catalyst surface, resulting in a high HYD/DDO ratio. But at a very high hydrogen pressure, the adsorbed hydrogen on the catalyst surface reached to a saturated value, which would lead to no or little effect on the conversion or product distribution. For example, Joshi et al. [44] had found that the *4*-propylguaiacol conversion remained constant after the hydrogen partial pressure 2.20 MPa. In summary, in this selected pressure range, high hydrogen pressure favored the high conversion and HYD route while low hydrogen pressure promoted the DDO route.

2.6. Catalytic reaction mechanism

Theoretically, the HDO of phenolic compounds proceeds with two main pathways: DDO and HYD, which are mainly attributed to the different adsorption modes on the active site: (i) vertical orientation adsorption and (ii) co-planar position adsorption. For DDO route, *p*-cresol was adsorbed on the active site of Ni–Mo–S catalyst via the donation of lone electron pair from the oxygen and then the hydrogen attacked on the $C_{aromatic}$—O bond to produce toluene [45]. As shown in Fig. 3b, in the last 2 h, the conversion had already reached to 100%, but the selectivity of toluene yielded by DDO route only decreased by 0.8%. In other words, the conversion of toluene at the end of 2 h run is less than 1.0%. In addition, with the presence of *p*-cresol, the hydrogenation of toluene was much slower due to the competitive adsorption of *p*-cresol and toluene on the catalyst surface [18]. Hence, in the HDO of *p*-cresol on these Ni–Mo–S catalysts, the hydrogenation of toluene could be neglected. For HYD route, *p*-cresol was adsorbed on the active site of Ni–Mo–S catalyst through the π-electrons of the aromatic ring followed by hydrogenation of the aromatic ring to produce *4*-methylcyclohexanol [39]. Then, *p*-cresol HDO transferred into *4*-methylcyclohexanol HDO. Free hydrogen adsorbed on Mo-based sulfide catalysts attacked the oxygen atom of *4*-methylcyclohexanol and eliminated H_2O to generate carbanion, and then accepted the free hydrogen to produce methylcyclohexane or generated a new double bond to form *4*-methylcyclohexene that was further hydrogenated to methylcyclohexane [46]. This reaction scheme is different from that over Ni–W–B amorphous catalysts and Pt supported catalysts [19,47], in which only HYD reaction route is proposed because of their high hydrogenation activity.

To explain the active sites of Ni(Co)-Mo(W)-S catalysts, several models such as Rim-Edge model, Edge decoration model

Table 3
Key reactions selected to evaluate the thermodynamic of *p*-cresol HDO.

Reaction	Equation	Temperature (°C) (ΔG, kcal/mol)			
		250	275	300	325
R1, HDO conversion of *p*-cresol to toluene	*p*-Cresol + H_2 = toluene + H_2O	−12.5	−11.7	−10.8	−10.0
R2, hydrogenation of *p*-cresol	*p*-Cresol + $3H_2$ = 4-methylcyclohexanol	−3.0	−0.7	1.5	3.8
R3, HDO conversion of *p*-cresol to 3-methylcyclohexene	*p*-Cresol + $3H_2$ = 3-methylcyclohexene + H_2O	−8.0	−6.1	−4.2	−2.3
R4, HDO conversion of *p*-cresol to methylcyclohexane	*p*-Cresol + $4H_2$ = methylcyclohexane + H_2O	−6.6	−3.0	0.7	4.3
R5, hydrogenation of toluene	Toluene + $3H_2$ = methylcyclohexane	−0.5	1.9	4.3	6.7
R6, hydrogenation of 3-methylcyclohexene	3-Methylcyclohexene + H_2 = methylcyclohexane	−2.4	1.243	5.2	9.4

and Remote control model had been proposed. Rim-Edge model describes MoS_2 catalyst as stacks of several discs. The top and bottom discs are defined as rim sites and the discs between the top and bottom discs are defined as edge sites. However, Wu et al. [48] had reported that Rim-Edge model was not suitable to explain the active sites for the HDO reaction of *p*-cresol because of the “steric hindrance” effect. Edge decoration model claimes that there generates Ni–Mo–S phase in the Ni promoted MoS_2 catalyst and the high catalytic activity is attributed to the formation of Ni–Mo–S active phase [28,49,50]. Recently, Yoosuk et al. [27] had reported that the maximum synergetic effect of Ni–Mo–S amorphous catalyst in the HDO of phenol was attributed to the higher dispersion of active species and the generation of more active Ni–Mo–S phase. However, Edge decoration model might be not very accurate in this study because it was hard to determine whether there really existed Ni–Mo–S phase or not during HDO reaction. But the characterization results showed that there appeared some Ni sulfides in the catalyst, which suggested that there might only exist separate Ni and Mo sulfides in the prepared catalysts and the high activity of Ni–Mo–S might be attributed to the synergistic effect of MoS_2 and Ni sulfides. To verify this conjecture, we prepared MoS_2–NiS with the same Ni/(Ni + Mo) molar ratio as that in Ni–Mo–0.3 by two-step hydrothermal method and then applied it into the HDO of *p*-cresol. MoS_2–NiS catalyst was prepared as following. Firstly, the mixed solution containing ammonium heptamolybdate and thiourea was added into a reactor and heated at 200 °C for 12 h. Secondly, nickel nitrate and thiourea were added into the reactor and heated at 200 °C for 12 h. The XRD and HRTEM characterization results of MoS_2–NiS are shown in Fig. 6. The peaks at $2\theta = 14°$, 33°, 39° and 59° were corresponded to MoS_2 while the peaks at $2\theta = 27°$, 31°, 35°, 38°, 45° and 53° were attributed to NiS_2. Two groups of parallel dark thread-like fringes could be observed from the HRTEM image of MoS_2–NiS, where the one group with a distance of 0.65 nm characterized the MoS_2 while the other group with a distance of 0.26 nm represented NiS_2. It also displayed that NiS_2 homogeneously dispersed on the surface of MoS_2.

Fig. 7a and b shows concentration changes of *p*-cresol and product versus reaction time on MoS_2–NiS and Ni–Mo–0.3 under the conditions of 3.0 MPa and 300 °C. After 5 h, *p*-cresol conversion on MoS_2–NiS was 99.5% with none oxygenated compounds, being much higher than that on Ni–Mo–0.3 (76.5%). According to the preparation method for MoS_2–NiS, it was very clear that MoS_2 was prepared firstly and then NiS_2 precipitated on the surface of MoS_2. In this case, Ni–Mo–S phase was hard to form. Moreover, we also prepared MoS_2 + NiS catalyst by physically mixing separately prepared MoS_2 and NiS_2 and tested its HDO activity, as shown in Fig. 7c. *p*-Cresol conversion was 92.0%, which was higher than that on Ni–Mo–0.3 but lower than that on MoS_2–NiS at the same reaction conditions. The higher HDO activity of MoS_2–NiS than MoS_2 + NiS resulted from the more uniform distribution of NiS_2 on MoS_2 in MoS_2–NiS. These indicated that the high activity of Ni promoted MoS_2 catalyst was attributed to the synergistic effect of MoS_2 and NiS_2 rather than the formation of Ni–Mo–S active phase. According to the reports by Gil-Llambías et al. [29,30], the synergistic effect could be well explained by the RC model through a migration of hydrogen spillover. Hydrogen spillover was generated on NiS_2 (donor), by the dissociation of molecular species (H_2) which migrated to the active phase of MoS_2 (acceptor). If NiS_2 on the catalyst surface was more, the hydrogenation product would be higher, but excess NiS_2 would cover some MoS_2 active sites, inhibiting the adsorption of *p*-cresol, leading to a reduction on conversion. Therefore, an optimal balance between NiS_2 and MoS_2 ensured a high HDO activity of Ni–Mo–S.

For Mo-based sulfides catalyst, it had reported that its activity did not directly depend on the surface area [27,39]. According to the HDO of *p*-cresol on Ni–Mo–S with different Ni/(Ni + Mo) ratio, the results in this study seemed to support this conclusion. As shown in Table 2, the reaction rate constant (k) for Mo–S with a surface area of 79.8 m^2/g [1.2×10^{-2} mL/(s g catalyst)] is lower than Ni–Mo–0.3

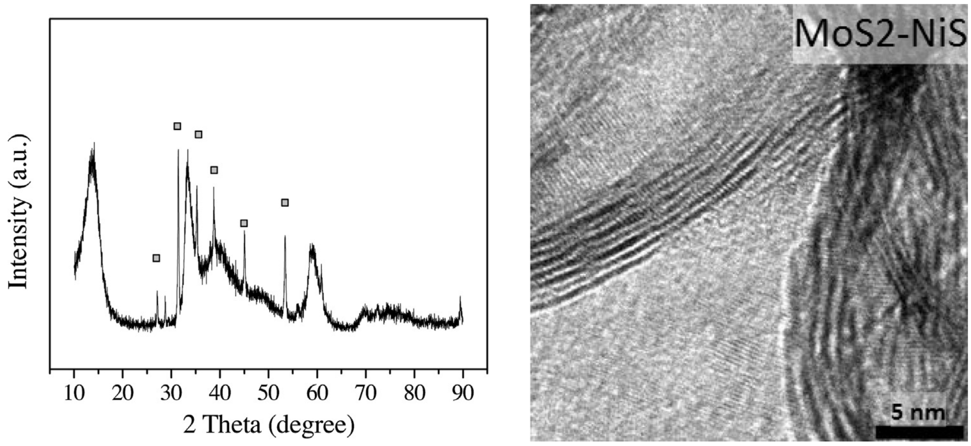

Fig. 6. XRD pattern and TEM image of MoS_2–NiS catalyst.

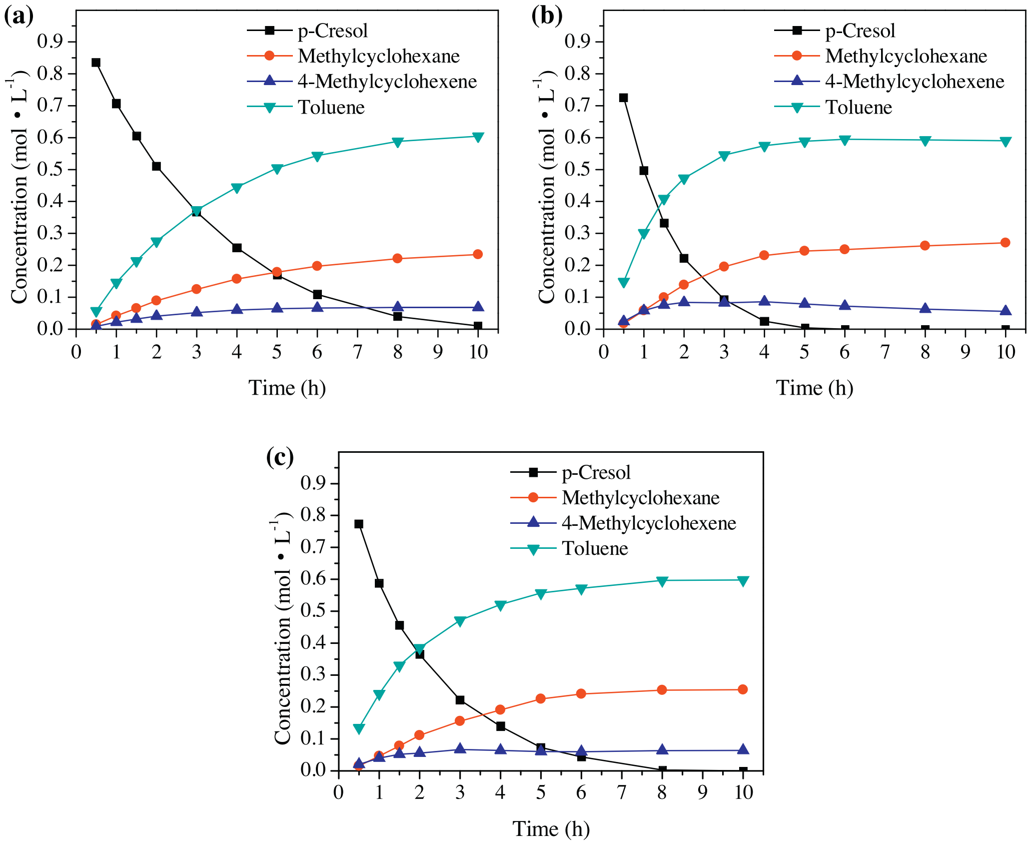

Fig. 7. The concentration changes of *p*-cresol and product versus reaction time on Ni–Mo–0.3 (a), MoS_2–NiS (b) and MoS_2 + NiS (c). Reaction condition: pressure 3.0 MPa, temperature 300 °C, stirring rate 900 r/min.

with a surface area of 16.3 m^2/g [3.2×10^{-2} mL/(s g catalyst)]. Nevertheless, these catalysts contained different active constituents, leading to different surface areas. There lacked evidence for the activity comparison of catalyst with the same active constituents but different surface area. Here, we compared Ni–Mo–0.3 with MoS_2–NiS on the catalytic activity. These two catalysts had the same Ni/(Ni + Mo) mole ratio but different surface area. The above discussion showed that the activity for Ni–Mo–*X* catalysts was decreased above a certain threshold nickel concentration level because of the coverage of active sites by NiS_2. According to this, MoS_2–NiS would have lower catalytic activity than that of Ni–Mo–0.3 because the XRD and HRTEM results shows that Ni sulfide on MoS_2–NiS surface was much more than that on Ni–Mo–0.3. However, MoS_2–NiS with a surface area of 84.3 m^2/g exhibited much higher HDO activity than Ni–Mo–0.3. Obviously, surface area also influenced the catalytic activity. Although the Ni sulfide on MoS_2–NiS catalyst surface was very high, covering many active sites, its large surface area exposed more available active sites. Consequently, the surface area also contributed to the activity of Mo-based sulfide catalyst in the HDO reaction, but it was not the decisive factor. Recent studies had also reported the similar results. For instance, Li et al. [51] had claimed that the excellent lithium storage property of MoS_2 was attributed to its large specific surface that could provide a large number of reaction sites. We had also demonstrated that the high HDO catalytic activity of MoS_2 catalyst depended on its large surface area while the product distribution depended on its morphology [52].

3. Conclusions

Unsupported Ni–Mo–S catalysts were prepared by hydrothermal method at low temperature (200 °C) and without H_2 or inert gas. With increasing Ni content in the Ni–Mo–S catalyst, the surface area decreased from 79.8 m^2/g for Mo–S to 10.7 m^2/g for Ni–Mo–0.5, and some of Ni sulfide was detected when the Ni/(Ni + Mo) molar ratio was above 0.3. In the HDO of *p*-cresol, the conversion on Ni–Mo–0.3 reached to 99.9% with a deoxygenation of 99.8% at 300 °C and 4.0 MPa hydrogen pressure for 6 h, which showed much higher catalytic activity than traditional Ni–Mo–S/γ-Al_2O_3 catalyst. The reaction rate constant k increased firstly and then decreased with the increase of Ni/(Ni + Mo) molar ratio. The HYD route yielding methylcyclohexane was enhanced as temperature increased to 300 °C, and then inhibited when further increasing the temperature. In the selected pressure range (2.0–4.0 MPa), both the conversion and HYD selectivity were improved with the increase of hydrogen pressure. Compared Ni–Mo–S catalyst prepared by one step with MoS_2–NiS and MoS_2 + NiS, the high HDO activity of Ni promoted MoS_2 catalyst depended on the synergistic effect of MoS_2 and NiS_2 rather than the formation of Ni–Mo–S active phase. This synergistic effect was well explained by the RC model through a migration of hydrogen spillover. An optimal balance between NiS_2 and MoS_2 leaded to the maximum HDO activity. The surface area also influenced the HDO activity of Mo-based sulphide catalysts.

Acknowledgements

This research was supported by the National Natural Science Foundation of China (Nos. 21306159, 21376202), Specialized research Fund for the Doctoral Program of Higher Education (20124301120009) and Natural Science Foundation of Hunan Province (13JJ4048).

References

[1] T.P. Vispute, H. Zhang, A. Sanna, R. Xiao, G.W. Huber, Science 330 (2010) 1222–1227.
[2] H. Wang, J. Male, Y. Wang, ACS Catal. 3 (2013) 1047–1070.
[3] E. Furimsky, Catal. Today 217 (2013) 13–56.
[4] J. Zakzeski, P.C.A. Bruijnincx, A.L. Jongerius, B.M. Weckhuysen, Chem. Rev. 110 (2010) 3552–3599.
[5] A.R. Ardiyanti, A. Gutierrez, M.L. Honkela, A.O.I. Krause, H.J. Heeres, Appl. Catal. A: Gen. 407 (2011) 56–66.
[6] M. Grilc, B. Likozar, J. Levec, Appl. Catal. B: Environ. 150–151 (2014) 275–287.
[7] M.A. Peralta, T. Sooknoi, T. Danuthai, D.E. Resasco, J. Mol. Catal. A: Chem. 312 (2009) 78–86.
[8] I.D. Mora, E. Méndez, L.J. Duarte, S.A. Giraldo, Appl. Catal. A: Gen. 474 (2014) 59–68.
[9] M.S. Zanuttini, B.O. Dalla Costa, C.A. Querini, M.A. Peralta, Appl. Catal. A: Gen. 482 (2014) 352–361.
[10] Y. Hong, H. Zhang, J. Sun, K.M. Ayman, A.J.R. Hensley, M. Gu, M.H. Engelhard, J.-S. McEwen, Y. Wang, ACS Catal. 4 (2014) 3335–3345.
[11] W. Wang, K. Zhang, Z. Qiao, L. Li, P. Liu, Y. Yang, Catal. Commun. 56 (2014) 17–22.
[12] X. Zhang, T. Wang, L. Ma, Q. Zhang, Y. Yu, Q. Liu, Catal. Commun. 33 (2013) 15–19.
[13] W. Wang, K. Zhang, H. Liu, Z. Qiao, Y. Yang, K. Ren, Catal. Commun. 41 (2013) 41–46.
[14] R. Olcese, M.M. Bettahar, B. Malaman, J. Ghanbaja, L. Tibavizco, D. Petitjean, A. Dufour, Appl. Catal. B: Environ. 129 (2013) 528–538.
[15] R.N. Olcese, J. Francois, M.M. Bettahar, D. Petitjean, A. Dufour, Energy Fuels 27 (2013) 975–984.
[16] X. Kong, W. Lai, J. Tian, Y. Li, X. Yan, L. Chen, ChemCatChem 5 (2013) 2009–2014.
[17] B. Yoosuk, D. Tumnantong, P. Prasassarakich, Chem. Eng. Sci. 79 (2012) 1–7.
[18] W. Wang, Y. Yang, H. Luo, T. Hu, W. Liu, Catal. Commun. 12 (2011) 436–440.
[19] W. Wang, Y. Yang, H. Luo, H. Peng, F. Wang, Ind. Eng. Chem. Res. 50 (2011) 10936–10942.
[20] V.N. Bui, D. Laurenti, P. Delichère, C. Geantet, Appl. Catal. B: Environ. 101 (2011) 246–255.
[21] V.M.L. Whiffen, K.J. Smith, Energy Fuels 24 (2010) 4728–4737.
[22] Y.Q. Yang, C.T. Tye, K.J. Smith, Catal. Commun. 9 (2008) 1364–1368.
[23] Q. Bu, H. Lei, S. Ren, L. Wang, Q. Zhang, J. Tang, R. Ruan, Bioresour. Technol. 108 (2012) 274–279.
[24] Q. Bu, H. Lei, S. Ren, L. Wang, J. Holladay, Q. Zhang, J. Tang, R. Ruan, Bioresour. Technol. 102 (2011) 7004–7007.
[25] Y. Yi, B. Zhang, X. Jin, L. Wang, C.T. Williams, G. Xiong, D. Su, C. Liang, J. Mol. Catal. A: Chem. 351 (2011) 120–127.
[26] C. Wang, Z. Wu, C. Tang, L. Li, D. Wang, Catal. Commun. 32 (2013) 76–80.
[27] B. Yoosuk, D. Tumnantong, P. Prasassarakich, Fuel 91 (2012) 246–252.
[28] H. Topsøe, B.S. Clausen, R. Candia, C. Wivel, S. Mørup, J. Catal. 68 (1981) 433–452.
[29] M. Villarroel, P. Baeza, N. Escalona, J. Ojeda, B. Delmon, F.J. Gil-Llambías, Appl. Catal. A: Gen. 345 (2008) 152–157.
[30] P. Baeza, M. Villarroel, P. Ávila, A. López Agudo, B. Delmon, F.J. Gil-Llambías, Appl. Catal. A: Gen. 304 (2006) 109–115.
[31] P. Baeza, M.S. Ureta-Zañartu, N. Escalona, J. Ojeda, F.J. Gil-Llambías, B. Delmon, Appl. Catal. A: Gen. 274 (2004) 303–309.
[32] F.J. Gil-Llambías, H. Rodríguez, I. Bouyssieres, M. Escudey, I. Carkovic, J. Catal. 102 (1986) 37–42.
[33] H. Topsøe, B.S. Clausen, Appl. Catal. 25 (1986) 273–293.
[34] M. Karroua, H. Matralis, P. Grange, B. Delmon, J. Catal. 139 (1993) 371–374.
[35] E. Furimsky, Appl. Catal. A: Gen. 199 (2000) 147–190.
[36] M. Polyakov, M. Poisot, M.W.E. van den Berg, T. Drescher, A. Lotnyk, L. Kienle, W. Bensch, M. Muhler, W. Grünert, Catal. Commun. 12 (2010) 231–237.
[37] D. Mondal, G. Villemure, G. Li, C. Song, J. Zhang, R. Hui, J. Chen, C. Fairbridge, Appl. Catal. A: Gen. 450 (2013) 230–236.
[38] M. Chhowalla, G.A.J. Amaratunga, Nature 407 (2000) 164–167.
[39] B. Yoosuk, J.H. Kim, C. Song, C. Ngamcharussrivichai, P. Prasassarakich, Catal. Today 130 (2008) 14–23.
[40] O.I. Şenol, E.M. Ryymin, T.R. Viljava, A.O.I. Krause, J. Mol. Catal. A: Chem. 277 (2007) 107–112.
[41] Y. Romero, F. Richard, S. Brunet, Appl. Catal. B: Environ. 98 (2010) 213–223.
[42] V.L. Whiffen, K. Smith, Top. Catal. 55 (2012) 981–990.
[43] F. Faglioni, W.A. Goddard, J. Chem. Phys. 122 (2005) 014704–014718.
[44] N. Joshi, A. Lawal, Ind. Eng. Chem. Res. 52 (2013) 4049–4058.
[45] W.Y. Wang, Y.Q. Yang, J.G. Bao, H.A. Luo, Catal. Commun. 11 (2009) 100–105.
[46] F.E. Massoth, P. Politzer, M.C. Concha, J.S. Murray, J. Jakowski, J. Simons, J. Phys. Chem. B 110 (2006) 14283–14291.
[47] C. Zhao, Y. Kou, A.A. Lemonidou, X. Li, J.A. Lercher, Angew. Chem. Int. Ed. 48 (2009) 3987–3990.
[48] C. Wang, D. Wang, Z. Wu, Z. Wang, C. Tang, P. Zhou, Appl. Catal. A: Gen. 476 (2014) 61–67.
[49] H. Farag, Appl. Catal. B: Environ. 84 (2008) 1–8.
[50] H. Topsøe, B.S. Clausen, Catal. Rev. 26 (1984) 395–420.
[51] X. Wang, Z. Zhang, Y. Chen, Y. Qu, Y. Lai, J. Li, J. Alloys Compd. 600 (2014) 84–90.
[52] W. Wang, K. Zhang, Z. Qiao, L. Li, P. Liu, Y. Yang, Ind. Eng. Chem. Res. 53 (2014) 10301–10309.